

Published in final edited form as:

Appl Math Comput. 2012 February 15; 218(12): 6841–6850. doi:10.1016/j.amc.2011.12.057.

Removal of malaria-infected red blood cells using magnetic cell separators: A computational study

Jeongho Kim⁽¹⁾, Mehrdad Massoudi⁽²⁾, James F. Antaki⁽¹⁾, and Alberto Gandini⁽¹⁾

⁽¹⁾Department of Biomedical Engineering, Carnegie Mellon University, Pittsburgh, PA, 15213 USA

⁽²⁾U. S. Department of Energy, National Energy Technology Laboratory (NETL), P. O. Box 10940, Pittsburgh, PA, 15236 USA

Abstract

High gradient magnetic field separators have been widely used in a variety of biological applications. Recently, the use of magnetic separators to remove malaria-infected red blood cells (pRBCs) from blood circulation in patients with severe malaria has been proposed in a dialysis-like treatment. The capture efficiency of this process depends on many interrelated design variables and constraints such as magnetic pole array pitch, chamber height, and flow rate. In this paper, we model the malaria-infected RBCs (pRBCs) as paramagnetic particles suspended in a Newtonian fluid. Trajectories of the infected cells are numerically calculated inside a micro-channel exposed to a periodic magnetic field gradient. First-order stiff ordinary differential equations (ODEs) governing the trajectory of particles under periodic magnetic fields due to an array of wires are solved numerically using the 1st–5th order adaptive step Runge-Kutta solver. The numerical experiments show that in order to achieve a capture efficiency of 99% for the pRBCs it is required to have a longer length than 80 mm; this implies that in principle, using optimization techniques the length could be adjusted, i.e., shortened to achieve 99% capture efficiency of the pRBCs.

Keywords

cell separator; red blood cells (RBC); malaria; microfluidics; magnetic forces; particle trajectory; micro-channel

1. Introduction

Malaria is a parasitic disease transmitted by the bite of an infected mosquito, which afflicts 300 to 500 million people, consuming 40% of the health expenditures of over 100 countries. The malaria parasite lives by feeding off the hemoglobin. To avoid death from the toxic hemoglobin's "heme", the parasite converts it into an insoluble highly compacted crystal known as hemozoin. Since each heme contains one atom of iron, the hemozoin becomes paramagnetic [1–4]. Studies of Paul et al. [5] have shown that malaria infected red blood cells (pRBCs), which contain the parasite and the hemozoin, behave like paramagnetic particles in a magnetic field. This discovery has motivated investigation of magnetic cell separation to isolate *in-vitro* grown malaria-infected cells from the whole blood [5–10].

Publisher's Disclaimer: This is a PDF file of an unedited manuscript that has been accepted for publication. As a service to our customers we are providing this early version of the manuscript. The manuscript will undergo copyediting, typesetting, and review of the resulting proof before it is published in its final citable form. Please note that during the production process errors may be discovered which could affect the content, and all legal disclaimers that apply to the journal pertain.

Recently, the magnetic separation of malaria-infected red blood cells (RBCs) from blood circulation in patients with severe malaria has been proposed in a dialysis-like treatment - known as the mPharesis™ system (Fig. 1). In severe malaria, 5% or higher (up to 60% in worst cases) of the patient's red blood cells (RBCs) may be infected [11]. Even when optimally treated, severe malaria results in mortality rates of 15%–22% [12, 13]. When available, blood exchange transfusion and erythropheresis have been effectively used to significantly accelerate the clearance of parasites - so that intravenous drug therapies may be more efficacious [14–19]. Unfortunately, current exchange transfuser (ET) and electrophoresis (EP) systems used in these treatments are not engineered to selectively separate the infected RBCs (pRBCs) from healthy RBCs, and consequently result in the consumption of donor blood up to 95% greater than necessary, increasing cost and the risks of transfusion trauma. The mPharesis™ system (Figure 1) - a patent-pending technology [20] - developed by Tropical Health Systems, LLC and Carnegie Mellon University targets the pRBCs based on their unique magnetic properties. It represents the first medical device of its kind to employ magnetic separation technology [19, 21] to clear these toxic cells from circulation. This study was conducted to determine optimal parameters of such a device.

Cell separation has been considered as a key element in the diagnosis and treatment of human disease; it is an initial step for further experimental analyses to disclose more information about the disease. However, manipulating of a cell still is a challenging task. The main needs are to achieve higher performance, lower cost of cell isolation systems, and a novel technique to manipulate some of the cells. Kumar and Lykke [22] reviewed various cell separation techniques using cell properties such as cell density (centrifugation), cell size (sedimentation and filtration), and cell charge (magnetism). For example, centrifugation can generate density gradients and is widely used for cell separation. Other separation techniques are based on surface properties (adherence and affinity) and functional properties (proliferation, phagocytosis, and antigen recognition). Among cell manipulation techniques, magnetic cell sorting has received more attention for cell separation. Melville et al. [23] showed erythrocytes can be isolated from other cells because of its different paramagnetic properties. Paul et al [5] used this principle to filtrate malaria-infected red blood cells from the whole blood. Magnetic forces are used to transport, position, isolate, and sort magnetic micro-/nano- particles as well as non-magnetic objects, i.e., diamagnetic particles in micro-fluidic systems.

In this paper, we report the use of numerical technique of the novel mPharesis™ dialysis-like device for removal of malaria-infected, parasitized RBCs (pRBCs). These cells, known to exhibit a magnetic dipole moment, are modeled as paramagnetic particles suspended in a Newtonian fluid. Trajectories of the infected cells are numerically calculated inside a micro-channel exposed to a periodic magnetic gradient field. In Section 2, we briefly discuss the mechanics of a magnetic cell separator. In Section 3, we look at the mathematical formulation of forces acting on an idealized malaria infected RBC in a fluid, and in Section 4, we derive the equations of motion for a population of pRBCs flowing in a micro-channel subject to a magnetic field. Section 5 provides numerical simulations of particle trajectories for various cases. In addition, we have included the lift and Faxen forces in the particle equation; these terms are normally ignored. With the approach taken in this study, we can easily determine the dimensions of the microchannel, the size of the magnetic wire, the pitch, etc.

2. The mechanics of a magnetic cell separator

Inglis et al [24] discussed two methods of using high gradient magnetic (HGM) cell separation. One is to use the native susceptibility of cells and effectively separate the RBCs from the whole blood. Han et al. [25] showed the continuous separation of red and white

blood cells (WBCs) in microdevices. They considered the three-stage cascade micro-separator on order to increase the efficiency of the separation of red and white blood cells, creating higher gradient magnetic fields [26]. Their experimental results showed that the three-stage cascade micro-separator achieved 93.5 % separation of red blood cells and 97.4 % of white blood cells while for the single-stage micro-separator, 91.1 % of red blood cells and 87.7 % of white blood cells were separated. A mathematical model indicated that deoxygenated RBCs can be separated from WBCs in plasma [27]. Zborowski et al. [28] considered deoxygenated and methHb-containing erythrocytes for cell separation. The other method is using magnetic beads where the specific cells which attach themselves to these magnetic beads are separated. Xia et al. [29] used HGMC-microfluidic separator to remove living *E. coli* bacteria (1×10^7 cells/ml) bound to 130 nm magnetic nanoparticles from phosphate buffer solution (PBS) and saline containing a concentration of RBCs (2×10^9 cells/ml). They introduced a triangular saw-tooth configuration to create high gradient magnetic fields. Shinha et al. [30] compared numerical prediction with measured data for magnetic particle trajectories and showed a very good agreement where they introduced a dimensionless ratio of the magnetic and the drag forces determining the capture efficiency of particles. Chen et al. [31] and Brandl et al. [32] have developed detoxification systems as a therapeutic tool for selective and rapid removal of biohazards using a magnetic separator. Convection-diffusion equations governing the concentration of magnetic beads have been integrated with numerical models for cell separation system (Mikkelsen and Bruus [33] and Li et al. [34]. Mohanty et al. [35]). Two good review papers on magnetic cell separation are Tonner and Irimia [36], and Pamme [37].

The mPharesis™ (magnetic aphaeresis) system operates similar to a dialysis machine, where the patient's peripheral blood is continuously withdrawn, purified, and returned to the circulation (Figure 1 top). The design of the mPharesis™ filter features a series of cascaded laminar flow channels (Figure 1 bottom) through which the infected blood is transported and exposed to a high magnetic field gradient (> 1000 Tesla/m). The latter is created by an array of micro-sized ferromagnetic structures, placed in close proximity to the blood, that creates a localize force field, causing the infected cells to migrate or "marginate," whereupon they are skimmed off by a side branch (bleed-slit, in Figure 1 bottom). A magnetic field is applied using a 0.3 Tesla permanent magnet adjacent to the array of micro-sized ferromagnetic structures. The purified blood is then returned to the patient from a return outlet, (C in Figure 1 bottom). This design allows continuous filtration, analogous to renal dialysis. The engineering challenge is to optimize the efficiency of this magnetic separator to maintain the overall size of the system within the desired envelope. The filtration efficiency of this device depends on many design variables and constraints such as magnetic pole array pitch, chamber height, and flow rate. In the next section we provide a brief review of the various forces acting on a particle flowing in a viscous fluid.

3. Mathematical formulation of forces acting on a particle in a fluid

Fluid dynamics of multiphase (or multi-component) problems employs two distinct approaches. In the *first* case, the amount of the dispersed component is so small that the motion of this component (usually referred to as the dispersed phase) does not greatly affect the motion of the continuous phase (the host fluid). This method is used extensively in applications such as atomization, sprays, and in flows where bubbles, droplets, and particles are treated as the dispersed phase. This approach is known as the *Dilute Phase* or the *Lagrangian* approach to particle studies. The *second* approach is employed when the two components interact to such an extent that each component directly influences the motion and the behavior of the other component. This is known as the *Dense Phase* approach, or the *Eulerian* (two-fluid) approach. This method is used extensively in fluidization, gas-solid

flows, pneumatic conveying, and suspensions. For a review and discussion of the relevant issues, see the two recent articles by Massoudi [38, 39].

To describe the behavior of particles suspended or entrained in a fluid, most researchers resort to the equation of motion of a single (spherical) particle in a fluid. Tchen [40] synthesized the work of Basset, Boussinesq, Stokes, and Oseen on the motion of a sphere settling under the force of gravity in a fluid at rest. The resulting force balance, sometimes known as the Basset-Boussinesq-Oseen (BBO) equation, is given by:

$$\frac{4\pi a^3}{3} \rho_p \dot{v}_p = -\frac{2\pi a^3}{3} \rho_f \dot{v}_p - 6\pi \mu_f a v_p - 6\pi \mu_f a \frac{a}{\sqrt{\pi} v_f} \int_{-\infty}^t \frac{\dot{v}_p(t_1)}{\sqrt{t-t_1}} dt_1 - \frac{4\pi a^3}{3} g(\rho_p - \rho_f) \tag{1}$$

where v_p is the velocity of the particle, ρ_f and ρ_p are density of the fluid and particle, respectively, a is the particle radius, g is the acceleration of gravity, μ_f and v_f are the dynamic viscosity and the kinematic viscosity of the fluid, respectively. The terms on the right-hand side of equation (1) reflect the presence of virtual mass, Stokes drag, Basset history effects, and buoyancy. Tchen (1947) modified equation (1) to describe the unsteady motion of a solid spherical particle in a fluid with a uniform flow field. His modifications include replacing the particle velocity by its relative velocity, and the addition of a term accounting for the pressure gradient in the fluid. The resulting expression is:

$$\frac{4\pi a^3}{3} \rho_p \dot{v}_p = \frac{4\pi a^3}{3} \rho_f \dot{v}_f - \frac{2\pi a^3}{3} \rho_f (\dot{v}_p - \dot{v}_f) - 6\pi \mu_f a (v_p - v_f) - 6\pi \mu_f a \frac{a}{\sqrt{\pi} v_f} \int_{-\infty}^t \frac{\dot{v}_p(t_1) - \dot{v}_f(t_1)}{\sqrt{t-t_1}} dt_1 - \frac{4\pi a^3}{3} g(\rho_p - \rho_f)$$

where v_f is the velocity of the fluid in the neighborhood of the particle but far enough away to be unaffected by it.

It should be noted that equation (2) is a scalar component of a more general vector equation. Corrsin and Lumley [41] argued that, for a nonuniform flow field, the full Navier-Stokes equations should be used to determine the pressure gradient. Buevich [42] criticized both previous studies by pointing out that adding a term to the BBO equation is not necessary. Soo [43, 44] argued that the pressure gradient force is exactly balanced by the fluid inertia forces and should not appear in the force balance in any form. The importance of the force due to the fluid pressure gradient is still a subject of study and disagreement [see Table 1]. Maxey and Riley [45], based on an analysis similar to that of Buevich, proposed the following equation for the force on a sphere in a nonuniform flow:

$$\begin{aligned} m_p \frac{dv_p}{dt} = & +m_f \frac{Dv_f}{Dt} |Y(t) \\ & -\frac{1}{2} m_f \frac{d}{dt} \{ \mathbf{v}_p(t) - \mathbf{v}_f[Y(t), t] - \frac{1}{10} a^2 \nabla^2 \mathbf{v}_f |Y(t) \} \\ & -6\pi a \mu_f \{ \mathbf{v}_p(t) - \mathbf{v}_f[Y(t), t] - \frac{1}{6} a^2 \nabla^2 \mathbf{v}_f |Y(t) \} \\ & +6\pi a^2 \mu_f \int_0^t d\tau \frac{(\frac{d}{d\tau} \{ \mathbf{v}_p(\tau) - \mathbf{v}_f[Y(\tau), \tau] - \frac{1}{6} a^2 \nabla^2 \mathbf{v}_f |Y(\tau) \})}{\sqrt{\pi} v_f(t-\tau)} \\ & + (m_p - m_f) \mathbf{g} \end{aligned} \tag{3}$$

It is noted that the inclusion of velocity gradients in their analysis results in modifications to the virtual mass, Stokes drag, and Basset history terms in order to account for the effect of a nonuniform flow field. These velocity gradients correspond to the physical effect known as Faxen forces (Happel and Brenner [46]).

Though equation (3) appears to be complete for a single particle in Stokes flow, there are, in general, other forces that must be considered - even for a purely mechanical system. For example, in flows with high relative velocity between phases, or large velocity gradients in

the fluid, lift may become an important effect (see McLaughlin [48], Ounis and Ahmadi [49]).

It is observed [50–52] that spheres in laminar Poiseuille flow through a pipe (at low Re) accumulate in an annulus some distance from the tube axis. Following the initial observations, a number of investigators verify this ‘tubular pinch’ effect and attempt to explain the lateral (or lift) force acting on the spheres. Though some authors attempt to explain the radial migrations in terms of particle spin (i.e., Magnus force), spheres prevented from spinning also reached equilibrium positions between wall and centerline. Saffman [53, 54] deduces that, since experimental results contradicted this conclusion, inertial effects must be involved. Saffman obtains the result for ‘slip-shear’ lift on a particle at low Reynolds number analogous to a result derived earlier for the ‘spin’ lift by Rubinow and Keller [55]. Saffman [53] includes particle spin in his analysis and shows that under circumstances where his results and Rubinow and Keller’s result strictly apply, the ‘shear’ lift dominates the ‘spin’ lift. The Saffman lift force is normal to the slip vector and the spin vector of the particle. If the particle lags the fluid, the lift will move the particle toward the faster adjacent fluid and vice versa if the particle leads the fluid. Ho and Leal [56] calculate another form of lift force on a single particle in a channel. This force is apparently a result of the wall effects. A detailed analysis, including experimental observation of lift forces in Couette systems is given by Halow and Wills [57, 58]. For an updated review of Saffman’s contribution to this field, we refer the reader to the recent article by Stone [59]. In majority of multiphase studies, lift forces are neglected. Massoudi [60] discusses the importance of these forces and through a simple order of magnitude analysis concludes that these forces, especially in the flows or in the regions of high velocity gradients (such as swirling flows), cannot be assumed to be negligible *a priori*. Massoudi [61] also provides a brief review of the interaction mechanisms. Ounis and Ahmadi [49] suggested the following equation:

$$\begin{aligned}
 m_p \frac{d\mathbf{v}_p}{dt} = & m_f \frac{D\mathbf{v}_f}{Dt} - \frac{1}{2} m_f \frac{d}{dt} \left(\mathbf{v}_p - \mathbf{v}_f - \frac{d^2}{40} \nabla^2 \mathbf{v}_f \right) \\
 & - 3\pi\mu_f d \left(\mathbf{v}_p - \mathbf{v}_f - \frac{d^2}{24} \nabla^2 \mathbf{v}_f \right) - \frac{3}{2} \pi d^2 \mu_f \int_0^t \frac{d}{d\tau} \left(\mathbf{v}_p - \mathbf{v}_f - \frac{d^2}{24} \nabla^2 \mathbf{v}_f \right) \frac{d\tau}{\sqrt{\pi\nu_f(t-\tau)}} \\
 & + \frac{K\pi d^2 (\rho_f \mu_f)^{1/2} \mathbf{D}_f}{3(\mathbf{D}_f : \mathbf{D}_f)^{1/4}} (\mathbf{v}_f - \mathbf{v}_p) + (m_p - m_f) \mathbf{g}
 \end{aligned} \tag{4}$$

where as before the subscripts f and p denote the fluid and the particle, respectively; \mathbf{v} is the velocity vector, t is time, μ_f is the dynamic viscosity, ν_f is the kinematic viscosity, m is the mass ($m = \frac{\pi}{6} d_p^3 \rho$), ρ is the density, d is the particle diameter ($=2a$), $K=2.594$ is the constant

coefficient of Saffman lift force, $\mathbf{D}_f = \frac{1}{2} \left[\nabla \mathbf{v}_f + (\nabla \mathbf{v}_f)^T \right]$, the time derivate for the moving

particle is $\frac{d\mathbf{v}_p}{dt} = \frac{\partial \mathbf{v}_p}{\partial t} + \mathbf{v}_p \frac{\partial \mathbf{v}_p}{\partial \mathbf{x}}$, the fluid acceleration is defined as $\frac{D\mathbf{v}_f}{Dt} = \frac{\partial \mathbf{v}_f}{\partial t} + \mathbf{v}_f \frac{\partial \mathbf{v}_f}{\partial \mathbf{x}}$, and $\mathbf{x}_p = x_p \mathbf{e}_x \sqcup y_p \mathbf{e}_y$. A generalized form of the Saffman shear lift force was proposed by Drew [62], Ahmadi [63], McTigue et al. [64]. Equation (4) is reduced to the lift force in a uniform shear field provided by Saffman [53, 54]. This form of the lift force is intended for Stokes flow regime and only valid for small particles. Also, spin of the particle is not taken into account in the above equations. In the next section, we look at a simplified case of magnetic particles flowing in a micro-channel subject to a magnetic field. The structure of this magnetic force is obtained from the work of Han et al. [65]. In reality, however, one must solve the Maxwell’s equations in conjunction with the equation of motion for the particles.

4. Flow of magnetic particles in a micro-channel

We consider a paramagnetic particle (representing the malaria-infected RBCs) in a steady fully-developed laminar flow between two plates (micro-channel). As the first approximation, we neglect the terms due to the pressure gradient, virtual mass, and Basset history force. However, we add a magnetic force on the right-hand side of equation 4. That is, only the Stokes drag, buoyancy, shear-lift and magnetic forces including the velocity gradients known Faxen force are considered. Thus equation (4) becomes:

$$m_p \frac{d\mathbf{v}_p}{dt} = -3\pi\mu_f d \left(\mathbf{v}_p - \mathbf{v}_f - \frac{d^2}{24} \nabla^2 \mathbf{v}_f \right) + (m_p - m_f) \mathbf{g} + \frac{K\pi d^2 (\rho_f \mu_f)^{1/2} \mathbf{D}_f}{3(\mathbf{D}_f : \mathbf{D}_f)^{1/4}} (\mathbf{v}_f - \mathbf{v}_p) + \mathbf{F}_{mag} \tag{5}$$

We also adopt the magnetic force derived by Han et al. [65] for a ferromagnetic cylindrical wire placed under a uniform magnetic field H_0 applied normal to the axis of the wire. However, unlike Han, which prescribed the direction of flow parallel to the longitudinal axis of the wire, the flow is taken here across the wire. (See Figure 2) The corresponding components of magnetic force in the Cartesian coordinates are given as:

$$\begin{aligned} \mathbf{F}_{mag} &= F_{mag,x}(x, y) \mathbf{e}_x + F_{mag,y}(x, y) \mathbf{e}_y \\ F_{mag,x}(x, y) &= \frac{-2k\mu_0(\chi_p - \chi_f)V_p a_w^2 H_0^2}{(x^2 + y^2)^3} [ka^2 + 3y^2 - x^2] x \\ F_{mag,y}(x, y) &= \frac{-2k\mu_0(\chi_p - \chi_f)V_p a_w^2 H_0^2}{(x^2 + y^2)^3} [ka^2 - 3x^2 + y^2] y \end{aligned} \tag{6}$$

where $k = \frac{\mu_w - \mu_0}{\mu_w + \mu_0}$, μ_w and μ_0 are the magnetic permeability of the ferromagnetic wire and free space respectively, χ_f and χ_p are the magnetic susceptibilities of the fluid solution and the paramagnetic particle (or pRBC), V_p is the volume of the paramagnetic particle (or pRBC); and a_w is the radius of the wire.

Let us consider an array of N_w wires located on the top of the permanent magnet shown in Figure 2. The center of the first wire is positioned at the origin of the x - y plane ($x=w_0=0$ and $y=0$), and all other wires are displayed side by side along the x -axis. The magnetic force distribution of the first wire ($n=1$) is given by Eq. 6. The center of the n th wire is located at $x=w_n$ and its magnetic force distribution can be written in terms of Eq. 6 as:

$$\mathbf{F}_{mag}^n(x, y) = \mathbf{F}_{mag}^1(x - w_n, y) \tag{7}$$

where we can label each conductor using the index $n=1, 2, 3, 4, \dots, N_w$. Therefore, we can define the total magnetic force distribution for the N_w array of wires by superposition:

$$\mathbf{F}_{mag}^{total}(x, y) = \sum_{n=1}^{N_w} \mathbf{F}_{mag}^1(x - w_n, y) \tag{8}$$

To solve Eq. 5, we need an expression for the fluid velocity \mathbf{v}_f in the micro-channel where flow is two-dimensional. It is known that the velocity profile for the flow between two plates is different from the flow through a channel (with side walls) with a square cross-section. In this problem, we assume a parabolic flow profile for a wide channel (width \gg height), where L denotes the length of the channel, and h_c and w_c denote the half-height and the half-width of the cross section as shown in Figure 2. For the fully developed pressure-driven steady flow between two fixed plates, the velocity is given as [66],

$$\mathbf{v}_f = -\frac{dp}{dx} \frac{h_c^2}{2\mu_f} \left[1 - \left(\frac{y - (a_w + h_c)}{h_c} \right)^2 \right] \mathbf{e}_x \tag{9}$$

where $\frac{dp}{dx}$ is the pressure drop and μ_f is the viscosity of a fluid, a_w and h_c are defined and shown in Figure 3. The volumetric flow rate Q is defined as $Q = A \bar{v}_f$ where the cross sectional area of the channel is $A = 4h_c w_c$. The average velocity \bar{v}_f is determined by integrating the velocity over the cross section, i.e., $\bar{v}_f = 1/A \int v_f dA = 2/3 v_{max}$. The maximum velocity v_{max} occurs at the centerline, $y = a + h_c$, i.e., $v_{max} = -(dp/dx)(h_c^2/2\mu_f)$.

Thus, the velocity profile can be rewritten as,

$$\mathbf{v}_f = \frac{3\bar{v}_f}{2} \left[1 - \left(\frac{y - (a_w + h_c)}{h_c} \right)^2 \right] \mathbf{e}_x \tag{10}$$

Finally, by substituting Eq. (8) and Eq. (10) into Eq. (5) we obtain the expression for the components of the forces acting on the particle. Thus the equations for a paramagnetic particle/RBC moving through the cell separator can be rewritten as:

$$\begin{aligned} m_p \frac{d v_{p,x}}{dt} = & -3\pi\mu_f d \left[v_{p,x} - \frac{3\bar{v}_f}{2} \left[1 - \left(\frac{y - (a_w + h_c)}{h_c} \right)^2 \right] \right] + \frac{d^2}{24} \frac{3\bar{v}_f}{h_c^2} \\ & + \frac{K\pi d^2 (\rho_f \mu_f)^{1/2}}{3(\mathbf{D}_f \cdot \mathbf{D}_f)^{1/4}} \left(\frac{3\bar{v}_f}{2h_c^2} [y - (a_w + h_c)] \right) v_{p,y} \\ & + \sum_{n=1}^{N_w} F_{mag,x}^1(x - w_n, y) \end{aligned} \tag{11}$$

and

$$\begin{aligned} m_p \frac{d v_{p,y}}{dt} = & -3\pi\mu_f d v_{p,y} - q_p (\rho_p - \rho_f) g \\ & + \frac{K\pi d^2 (\rho_f \mu_f)^{1/2}}{3(\mathbf{D}_f \cdot \mathbf{D}_f)^{1/4}} \left(\frac{3\bar{v}_f}{2h_c^2} [y - (a_w + h_c)] \right) \left(v_{p,x} - \frac{3\bar{v}_f}{2} \left[1 - \left(\frac{y - (a_w + h_c)}{h_c} \right)^2 \right] \right) \\ & + \sum_{n=1}^{N_w} F_{mag,y}^1(x - w_n, y) \end{aligned} \tag{12}$$

where $q_p \left(= \frac{4\pi a^3}{3} \right)$ is the volume of the particle and

$$\frac{dx_p}{dt} = v_{p,x} \tag{13}$$

$$\frac{dy_p}{dt} = v_{p,y} \tag{14}$$

and

$$\mathbf{D}_f \cdot \mathbf{D}_f = \frac{9\bar{v}_f^2}{2h_c^4} [y - (a_w + h_c)]^2 \tag{15}$$

Note that $\mathbf{v}_p = v_{p,x} \mathbf{e}_x + v_{p,y} \mathbf{e}_y$ at any position $\mathbf{x}_p = x_p \mathbf{e}_x + y_p \mathbf{e}_y$. In these expressions, $v_{p,x}$ and $v_{p,y}$ are the components of the particle velocity.

5. Numerical simulations and particle trajectories

Equations (11) – (14) represent a coupled system of first-order ordinary differential equations (ODEs) that are to be solved with appropriate initial conditions for the position $x_p(0), y_p(0)$, and the velocity $v_{p,x}(0)=v_f$, and $v_{p,y}(0)=0$ of the particle. These equations were solved numerically using the 1st–5th order adaptive step Runge-Kutta solver for stiff ODE systems (ode15s in MATLAB ODE solver). The relative and absolute error tolerances were set to 1e-5 and 1e-4 respectively. An alternative approach to simulate particle motion could be a discrete particle method when particle-fluid and particle-particle interactions are important.

The magnetic force in the y-direction is illustrated in Figure 3. (The x-axis is shifted by 50 micron to reference the magnetic force field in the channel.) A cubic regression to these results show that the force scales as $1/x^3$. The x-component of the magnetic force plotted in Figure 4, at $y=100$ micron illustrates an approximately sinusoidal fluctuation along the x-direction.

Figure 5 shows the trajectories of paramagnetic particles where Faxen and lift forces are included. It is observed that as the strength of the magnetic field decreases, the Faxen and the lift forces do not play a significant role on the motion of the particles. Therefore, the external magnetic flux was set to be 0.3 Tesla and we assumed that the Faxen and lift forces are negligible in the remainder of the numerical studies.

Figure 6 shows the trajectory of five ferromagnetic particles seeded at the entrance of the micro-channel, illustrating their deflection due to the magnetic force. The ferromagnetic particle has diameter of 0.3 micron and susceptibility of 0.26. The susceptibility of plasma is -7.7×10^{-6} . The numerical results also show that most of the particles are captured at the bottom of the channel near the wires within 13mm (for 1 cc/min) and 65mm (for 5 cc/min), thus suggesting a minimum length of the channel could be achieved by optimizing the design parameters.

Next we considered the malaria-infected red blood cells (pRBCs) with diameter of 8 micron and susceptibility of -6.2×10^{-6} (See Figure 7). The susceptibility of plasma is -7.7×10^{-6} . pRBC becomes paramagnetic due to its susceptibility with respect to plasma susceptibility. Some of the particles are not captured within the channel length of 75 mm for flow rates of 1 cc/min and 5 cc/min, since the infected RBCs are more paramagnetic than the ferromagnetic beads of the previous simulation. Paramagnetic particles are less deflected than the ferromagnetic particles by a permanent magnet. Paramagnetic substances have linear magnetization curves under normal circumstances and have no magnetism when the external magnetic field is removed, where the susceptibility is small and positive. Ferromagnetic magnetization curve is nonlinear. Its susceptibility is positive and large, which changes with H [67].

6. Concluding remarks

The main assumptions in our simulations of particle trajectory are: (1) no particle-particle interaction (no collisions); and (2) the behavior or the response of the particle is affected by the fluid motion whereas the fluid motion is unaffected by the presence of the particle, (one-way interaction). For a system of dense particles, these assumptions would not be valid. In most studies the forces due to pressure gradient and lift force are neglected; however it is known that the lift forces could be important in a small scale geometry [53, 60, 62, 68].

In this study, we have used the Lagrangian approach to study the particle trajectory while estimating design dimensions of the cell separation device. For a complete three dimensional geometry, we can use a Lagrangian-Eulerian CFD approach. However, these methods do not consider particle-particle interactions that can affect the cell aggregation and deformability of the cells. To better predict the phase separation of the RBCs and the plasma, one should consider alternative approaches such as the mixture theory [47, 60, 61, 69–71] or the particulate dynamics [72–74]. In this paper, we modeled the malaria infected RBCs (pRBCs) as paramagnetic particles suspended in a Newtonian fluid. Trajectories of the infected cells are numerically calculated inside a micro-channel exposed to a periodic magnetic field gradient. First order stiff ordinary differential equations (ODEs) governing particle's trajectory under periodic magnetic fields due to an array of wires were solved numerically using a the 1st–5th order adaptive step Runge-Kutta solver. The numerical experiments show that in order to achieve a capture efficiency of 99% for the pRBCs it is required to have a longer length than 80 mm; this implies that in principle, using optimization techniques the length could be adjusted, i.e., shortened to achieve 99% capture efficiency of the pRBCs.

For future study, we will consider more general cases using Eq. (4) for unsteady flow problems in complex geometries. We need to consider a 3-dimensional Lagrangian-Eulerian approach to investigate behavior of the pRBC in complex geometries where the magnetic field generated by a series of wires due to the external uniform field magnet also has to be considered using the Maxwell's equations. We will also perform numerical optimization studies on the height of the channel and the magnetic pitch.

Acknowledgments

This project was supported by NIH R01 HL089456-01.

References

1. Gligorijevic B, McAllister R, Urbach JS, Roepke PD. Spinning disk confocal microscopy of live, intraerythrocytic malarial parasites. 1. Quantification of hemozoin development for drug sensitive versus resistant malaria. *Biochemistry*. 2006; 45:12400–12410. [PubMed: 17029396]
2. Moore LR, Fujioka H, Williams PS, Chalmers JJ, Grimberg B, Zimmerman PA, Zborowski M. Hemoglobin degradation in malaria-infected erythrocytes determined from live cell magnetophoresis. *The FASEB journal*. 2006; 20:747–749. [PubMed: 16461330]
3. Hackett S, Hamzah J, Davis TE, St Pierre TG. Magnetic susceptibility of iron in malaria-infected red blood cells. *Biochimica et Biophysica Acta*. 2009; 1792:93–99. [PubMed: 19056489]
4. Zborowski M, Ostera GR, Moore LR, Milliron S, Chalmers JJ, Schechter AN. Red blood cell magnetophoresis. *Biophysical journal*. 2003; 84:2638–2645. [PubMed: 12668472]
5. Paul F, Roath S, Melville D, Warhurst DC, Osisanya JOS. Separation of malaria-infected erythrocytes from whole blood - Use of a selective high-gradient magnetic separation technique. *Lancet*. 1981; 2:70–71. [PubMed: 6113443]
6. Gascoyne P, Satayavivad J, Ruchirawat M. Microfluidic approaches to malaria detection. *Acta Trop*. 2004; 89:357–369. [PubMed: 14744562]
7. Zimmerman PA, Thomson JM, Fujioka H, Collins WE, Zborowski M. Diagnosis of malaria by magnetic deposition microscopy. *Am J Trop Med Hyg*. 2006; 74:568–572. [PubMed: 16606985]
8. Ribaut C, Berry A, Chevalley S, Reybier K, Morlais I, Parzy D, Nepveu F, Benoit-Vical F, Valentin A. Concentration and purification by magnetic separation of the erythrocytic stages of all human *Plasmodium* species. *Malar J*. 2008; 7:45. [PubMed: 18321384]
9. Ahn SY, Shin MY, Kim YA, Yoo JA, Kwak DH, Jung YJ, Jun G, Ryu SH, Yeom JS, Ahn JY, Chai JY, Park JW. Magnetic separation: a highly effective method for synchronization of cultured erythrocytic *Plasmodium falciparum*. *Parasitol Res*. 2008; 102:1195–1200. [PubMed: 18320226]

10. Bhakdi S, Ottinger A, Somsri S, Sratongno P, Pannadaporn P, Chamma P, Malasit P, Pattanapanyasat K, Neumann H. Optimized high gradient magnetic separation for isolation of Plasmodium-infected red blood cells. *Malar J.* 2010; 9:38. [PubMed: 20122252]
11. Trampuz A, Jereb M, Muzlovic I, Prabhu RM. Clinical review: severe malaria. *Critical Care.* 2003; 7:315–323. [PubMed: 12930555]
12. Omari AA, Garner P. Malaria: severe, life-threatening. *Clinical evidence.* 2007; 7:913.
13. Campagna AM, Patnaik MM. Advances in global biotechnology and local resources to treat malaria. *Minnesota medicine.* 2009; 92:44–45. [PubMed: 19331290]
14. Deshpande A, Kalgutkar S, Udani S. Red cell exchange using cell separator (therapeutic erythrocytapheresis) in two children with acute severe malaria. *Journal of Association of Physicians of India.* 2003; 51:925–926. [PubMed: 14710987]
15. Van Genderen PJJ, Hesselink DA, Bezemer JM, Wismans PJ, Overbosch D. Efficacy and safety of exchange transfusion as an adjunct therapy for severe Plasmodium falciparum malaria in nonimmune travelers: a 10 year single center experience with a standardized treatment protocol. *Transfusion.* 2010; 50:787–794. [PubMed: 19951317]
16. Shelat SG, Lott JP, Braga MS. Considerations on the use of adjunct red blood cell exchange transfusion in the treatment of severe Plasmodium falciparum malaria. *Transfusion.* 2010; 50:875–880. [PubMed: 20003050]
17. Boctor F, Diaz-Fuentes G, Mohandas K, Uehlinger J. Plasmodium falciparum and RBC exchange. *Transfusion.* 2003; 43:549–549. [PubMed: 12702171]
18. Boctor FN, Dorion RP. Malaria and hereditary elliptocytosis. *American Journal of Hematology.* 2008; 83:753–753. [PubMed: 17696197]
19. Phillips P, Nantel S, Benny WB. Exchange transfusion as an adjunct to the treatment of severe falciparum malaria: case report and review. *Review of Infectious Diseases.* 1990; 12:1100–1108.
20. Gandini, A.; Weinstein, R.; Parks, D.; Shaw, R. A Blood Purification Method and Apparatus for the Treatment of Malaria. Patent application number. 20100331753. 2009. www.uspto.gov
21. White NJ. What is the future of exchange transfusion in severe malaria? *Journal of Infection.* 1999; 39:185–186. [PubMed: 10714792]
22. Kumar RK, Lykke AWJ. Cell separation - A review. *Pathology.* 1984; 16:53–62. [PubMed: 6371684]
23. Melville D, Paul F, Roath S. Direct magnetic separation of red cells from whole blood. *Nature.* 1975; 255:706–706. [PubMed: 1134566]
24. Inglis DW, Riehn R, Sturm JC, Austin RH. Microfluidic high gradient magnetic cell separation. *J Appl Phys.* 2006; 99
25. Han KH, Frazier AB. Continuous magnetophoretic separation of blood cells in microdevice format. *J Appl Phys.* 2004; 96:5797–5802.
26. Han KH, Frazier AB. Paramagnetic capture mode magnetophoretic microseparator for high efficiency blood cell separations. *Lab Chip.* 2006; 6:265–273. [PubMed: 16450037]
27. Furlani EP. Magnetophoretic separation of blood cells at the microscale. *J Phys D-Appl Phys.* 2007; 40:1313–1319.
28. Zborowski M, Oстера GR, Moore LR, Milliron S, Chalmers JJ, Schechter AN. Magnetophoretic separation of red blood cells. *Abstr Pap Am Chem Soc.* 2003; 225:991.
29. Xia N, Hunt TP, Mayers BT, Alsberg E, Whitesides GM, Westervelt RM, Ingber DE. Combined microfluidic-micromagnetic separation of living cells in continuous flow. *Biomed Microdevices.* 2006; 8:299–308. [PubMed: 17003962]
30. Sinha A, Ganguly R, De AK, Puri IK. Single magnetic particle dynamics in a microchannel. *Phys Fluids.* 2007; 1910.1063/1061.2780191
31. Chen H, Bockenfeld D, Rempfer D, Kaminski MD, Rosengart AJ. Three-dimensional modeling of a portable medical device for magnetic separation of particles from biological fluids. *Phys Med Biol.* 2007; 52:5205–5218. [PubMed: 17762081]
32. Brandl M, Mayer M, Hartmann J, Posniecek T, Fabian C, Falkenhagen D. Theoretical analysis of ferromagnetic microparticles in streaming liquid under the influence of external magnetic forces. *J Magn Magn Mater.* 2010; 322:2454–2464.

33. Mikkelsen C, Bruus H. Microfluidic capturing-dynamics of paramagnetic bead suspensions. *Lab Chip*. 2005; 5:1293–1297. [PubMed: 16234954]
34. Li XL, Yao KL, Liu ZL. CFD study on the magnetic fluid delivering in the vessel in high-gradient magnetic field. *J Magn Magn Mater*. 2008; 320:1753–1758.
35. Mohanty S, Baier T, Schonfeld F. Three-dimensional CFD modelling of a continuous immunomagneto-phoretic cell capture in BioMEMs. *Biochemical Engineering Journal*. 2010; 51:110–116.
36. Toner M, Irimia D. Blood-on-a-chip. *Annu Rev Biomed Eng*. 2005; 7:77–103. [PubMed: 16004567]
37. Pamme N. Magnetism and microfluidics. *Lab Chip*. 2006; 6:24–38. [PubMed: 16372066]
38. Massoudi M. A note on the meaning of mixture viscosity using the classical continuum theories of mixtures. *International Journal of Engineering Science*. 2008; 46:677–689.
39. Massoudi M. A Mixture Theory formulation for hydraulic or pneumatic transport of solid particles. *International Journal of Engineering Science*. 2010; 48:1440–1461.
40. Tchen, CM. Mean value and correlation problems connected with the motion of small particles suspended in a turbulent fluid. *Martinus Nijhoff; The Hague*: 1947.
41. Corrsin S, Lumley J. On the equation of motion for a particle in turbulent fluid. *Applied Scientific Research*. 1956; 6:114–116.
42. Buevich YA. Motion resistance of a particle suspended in a turbulent medium. *Fluid Dynamics*. 1966; 1:119–119.
43. Soo SL. Equation of motion of a solid particle suspended in a fluid. *Phys Fluids*. 1975; 18:263.
44. Soo SL. Net effect of pressure gradient on a sphere. *Phys Fluids*. 1976; 19:757.
45. Maxey MR, Riley JJ. Equation of motion for a small rigid sphere in a nonuniform flow. *Phys Fluids*. 1983; 26:883.
46. Happel, J.; Brenner, H. *Low Reynolds number hydrodynamics*. Noordhoff Intl. Pub; Leiden: 1973.
47. Massoudi M, Rao CL. Vertical flow of a multiphase mixture in a channel. *Mathematical Problems in Engineering*. 2001; 6:505–526.
48. McLaughlin JB. Aerosol particle deposition in numerically simulated channel flow. *Physics of Fluids A: Fluid Dynamics*. 1989; 1:1211.
49. Ounis H, Ahmadi G. Motions of small rigid spheres in simulated random velocity field. *Journal of Engineering Mechanics*. 1989; 115:2107.
50. Segre G, Silberberg A. Radial particle displacements in Poiseuille flow of suspensions. *Nature*. 1961; 189:209–210.
51. Segre G, Silberberg A. Behaviour of macroscopic rigid spheres in Poiseuille flow 1. Determination of local concentration by statistical analysis of particle passages through crossed light beams. *Journal of Fluid Mechanics*. 1962; 14:115–135.
52. Segre G, Silberberg A. Behaviour of macroscopic rigid spheres in Poiseuille flow 2. Experimental results and interpretation. *Journal of Fluid Mechanics*. 1962; 14:136–157.
53. Saffman PG. Lift on a small sphere in a slow shear flow. *Journal of Fluid Mechanics*. 1965; 22:385–400.
54. Saffman PG. Correction. *Journal of Fluid Mechanics*. 1968; 31:624.
55. Rubinow SI, Keller JB. The transverse force on a spinning sphere moving in a viscous fluid. *Journal of Fluid Mechanics*. 1961; 11:447–459.
56. Ho BP, Leal LG. Inertial migration of rigid spheres in 2-dimensional unidirectional flows. *Journal of Fluid Mechanics*. 1974; 65:365–400.
57. Halow JS, Wills GB. Experimental observations of sphere migration in couette systems. *Industrial & Engineering Chemistry Fundamentals*. 1970; 9:603–607.
58. Halow JS, Wills GB. Radial migration of spherical particles in couette systems. *Aiche Journal*. 1970; 16:281–286.
59. Stone H. Philip Saffman and viscous flow theory. *Journal of Fluid Mechanics*. 2000; 409:165–183.
60. Massoudi M. On the importance of material frame-indifference and lift forces in multiphase flows. *Chemical Engineering Science*. 2002; 57:3687–3701.

61. Massoudi M. Constitutive relations for the interaction force in multicomponent particulate flows. *International Journal of Non-Linear Mechanics*. 2003; 38:313–336.
62. Drew DA. Two-phase flows: constitutive equations for lift and Brownian motion and some basic flows. *Archive for Rational Mechanics and Analysis*. 1976; 62:149–163.
63. Ahmadi G. A generalized continuum theory for granular materials. *International Journal of NonLinear Mechanics*. 1982; 17:21–33.
64. McTigue DF, Givler RC, Nunziato JW. Rheological effects of nonuniform particle distributions in dilute suspensions. *Journal of Rheology*. 1986; 30:1053.
65. Han KH, Frazier AB. Paramagnetic capture mode magnetophoretic microseparator for blood cells. *IEE Proc-Nanobiotechnol*. 2006; 153:67–73. [PubMed: 16948490]
66. White, FM. *Fluid Mechanics*. 4. McGraw-Hill; 1999.
67. Cullity, BD.; Graham, CD. *Introduction to magnetic materials*. Wiley-IEEE Press; 2008.
68. Eichhorn R, Small S. Experiments on the lift and drag of spheres suspended in a Poiseuille flow. *Journal of Fluid Mechanics*. 1964; 20:513–527.
69. Johnson G, Massoudi M, Rajagopal KR. Flow of a fluid-solid mixture between flat plates. *Chemical Engineering Science*. 1991; 46:1713–1723.
70. Massoudi M, Rajagopal KR, Phuoc TX. On the fully developed flow of a dense particulate mixture in a pipe. *Powder technology*. 1999; 104:258–268.
71. Massoudi M, Antaki JF. An anisotropic constitutive equation for the stress tensor of blood based on mixture theory. *Mathematical Problems in Engineering*. 2008; 2008:1155/2008/579172
72. Zhang J, Johnson PC, Popel AS. Effects of erythrocyte deformability and aggregation on the cell free layer and apparent viscosity of microscopic blood flows. *Microvascular Research*. 2009; 77:265–272. [PubMed: 19323969]
73. Veerapaneni SK, Gueyffier D, Zorin D, Biro G. A boundary integral method for simulating the dynamics of inextensible vesicles suspended in a viscous fluid in 2D. *J Comput Phys*. 2009; 228:2334–2353.
74. Jin Q, Verdier C, Singh P, Aubry N, Chotard-Ghodsnia R, Duperray A. Migration and deformation of leukocytes in pressure driven flows. *Mechanics Research Communications*. 2007; 34:411–422.

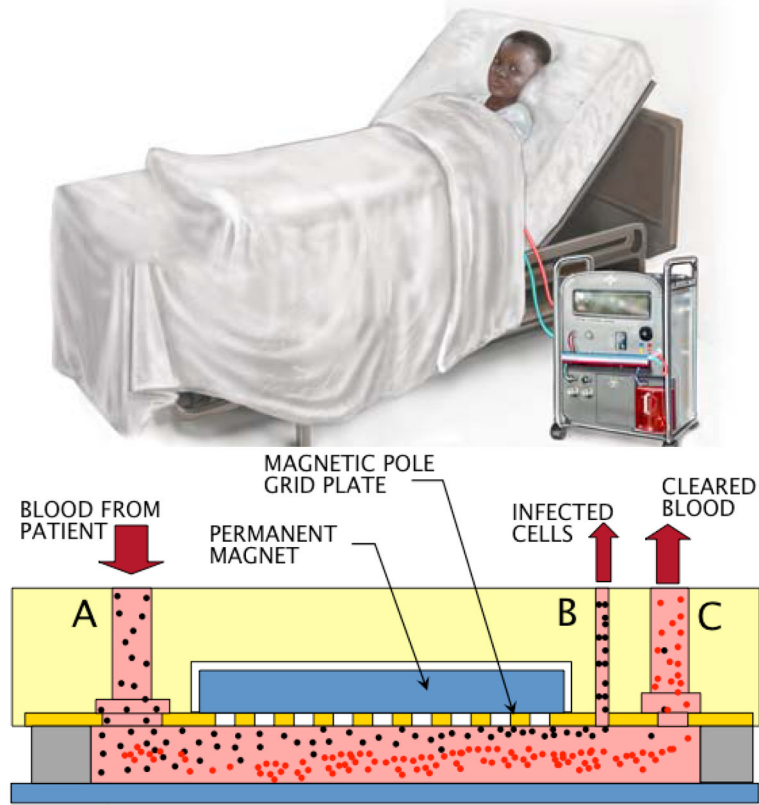


Figure 1. The direction of the flow and the magnetic field in the magnetic cell separator. The origin of the x - y plane is located at the center of the first wire with a diameter of a_w and each wire is displaced horizontally by the pitch (l_w). W_{n-1} is the x -directional displacement for the n^{th} wire. The magnetic force is distributed about a circular wire under a uniform magnetic

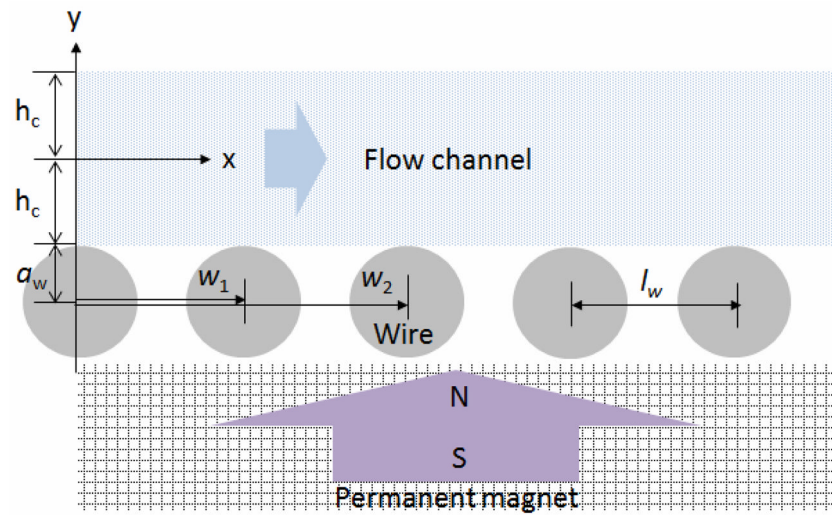


Figure 2. The direction of the flow and the magnetic field in the magnetic cell separator.

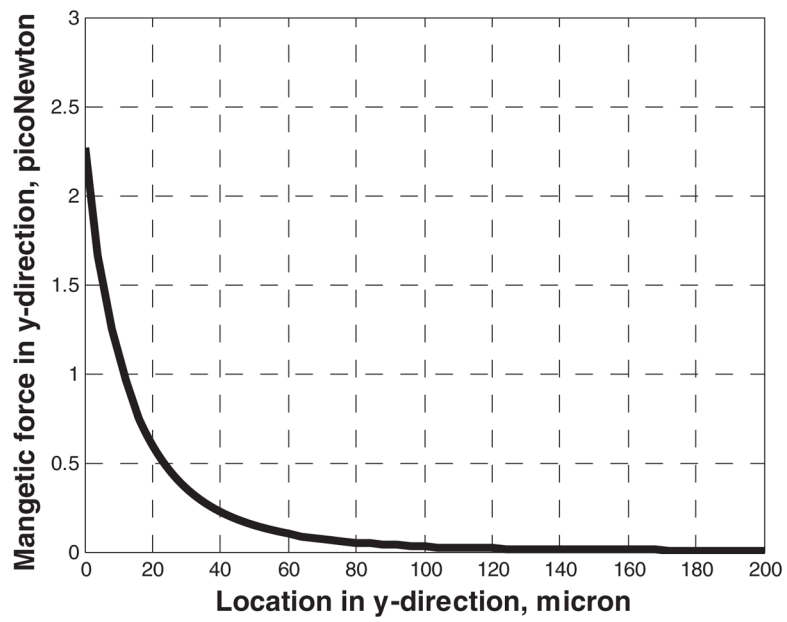


Figure 3.
The y component of the magnetic force along y direction from edge of the wire.

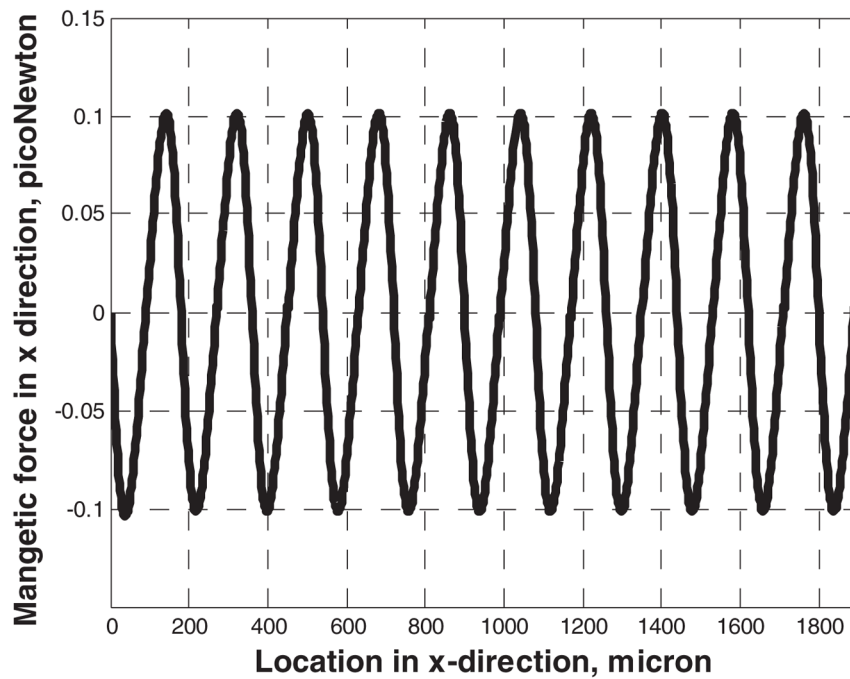


Figure 4.
The x component of the magnetic force along x direction at $y=100$ micron.

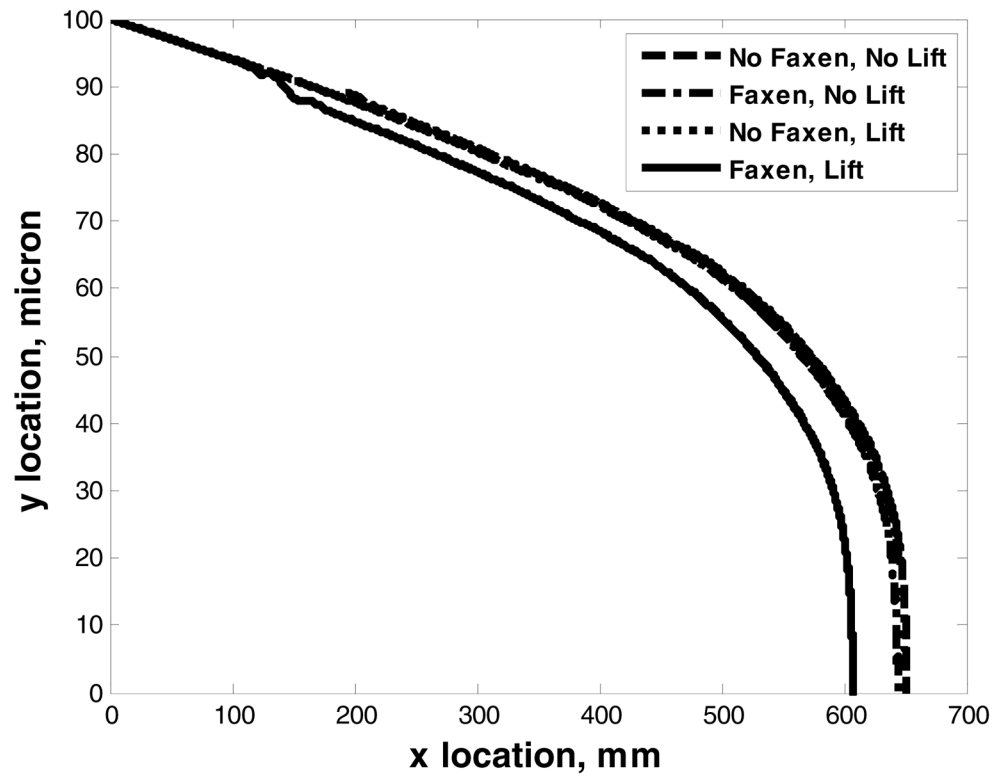


Figure 5. Plot of ferromagnetic bead trajectories at 5 cc flow rate and 0.05 Tesla magnetic flux at the particle seeding point of $x=0$, $y=100$ micron. The wire pitch (l_w) is 200 micron and the diameter of the wire (a_w) is 100 micron. The height of the micro-channel is 200 micron.

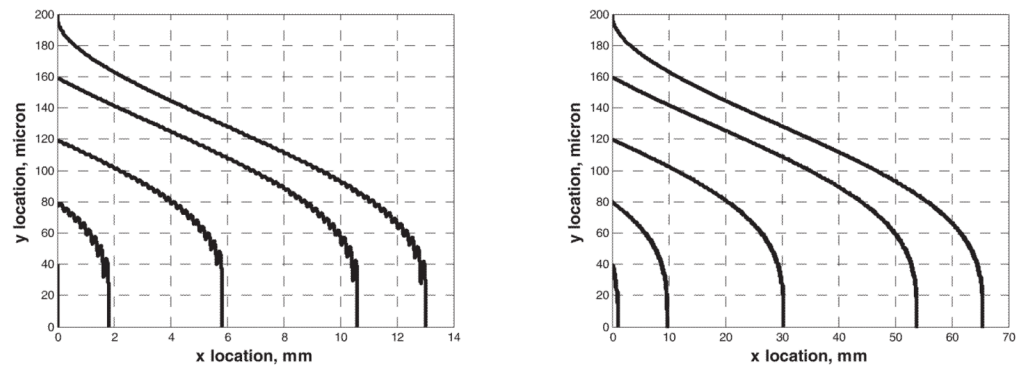


Figure 6.

Plot of ferromagnetic bead trajectories at 1 cc/min (left) and 5 cc/min (right) flow rate. The magnetic flux is 0.3 Tesla. The wire pitch (l_w) is 200 micron and the diameter of the wire (a_w) is 100 micron. The height of the micro-channel is 200 micron.

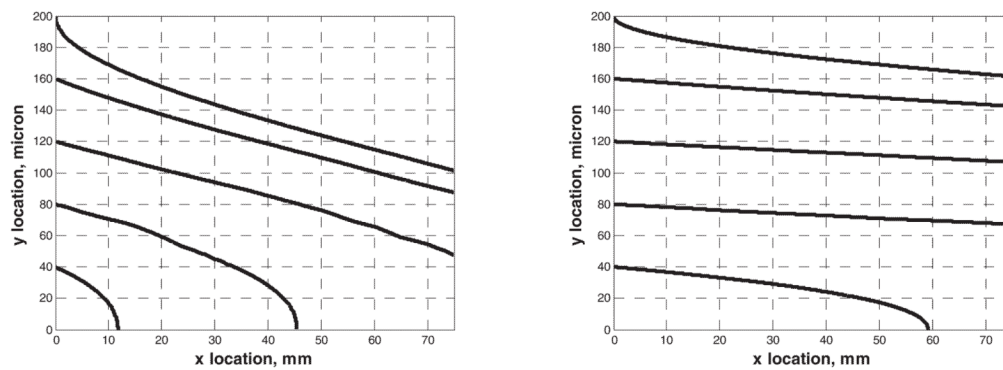


Figure 7. Plot of pRBC trajectories at 1 cc/min (left) and 5 cc/min (right) flow rate. The magnetic flux is 0.3 Tesla. The wire pitch (l_w) is 200 micron and the diameter of the wire (a_w) is 100 micron. The height of the micro-channel is 200 micron.

Table 1

Force due to pressure gradient [Massoudi and Rao 2001 [47]]

Author	Pressure Term
Tchen, 1947	$\frac{4\pi a^3}{3} \rho_f \left(\frac{\partial \mathbf{v}_p}{\partial t} + \mathbf{v}_p \frac{\partial \mathbf{v}_p}{\partial \mathbf{x}} \right)$
Corrsin and Lumley, 1956	$\frac{4\pi a^3}{3} \rho_f \left(\frac{\partial \mathbf{v}_p}{\partial t} + (\mathbf{grad} \mathbf{v}_p) \mathbf{v}_p - \nu \nabla^2 \mathbf{v}_p \right)$
Buevich, 1966	$\frac{4\pi a^3}{3} \rho_f \left(\frac{\partial \mathbf{v}_p}{\partial t} + (\mathbf{grad} \mathbf{v}_p) \mathbf{v}_f \right)$
Soo, 1975, 1976	0
Maxey and Riley, 1983	$\frac{4\pi a^3}{3} \rho_f \left(\frac{\partial \mathbf{v}_p}{\partial t} + (\mathbf{grad} \mathbf{v}_p) \mathbf{v}_p \right) \Big _{\mathbf{x}=\mathbf{y}(\mathbf{t})}$